

# Subsurface Tumor Ablation with Near-infrared Radiation using Intratumoral and Intravenous Injection of Nanoparticles

Anup Paul, Nanda Kishor Bandaru, Arunn Narasimhan and Sarit K. Das\*

Heat Transfer and Thermal Power Laboratory, Mechanical Engineering Department, IIT Madras, Chennai, Tamil Nadu, 600036

## ABSTRACT

Targeting nanoparticles to the tumor site is a salient feature for the tumor ablation during plasmonic photo-thermal therapy. Many of the safety considerations in surgical intervention suggest the alternative route of laser irradiation for photo-thermal destruction of tissues in presence of gold nanorods. The degree of tissue damage depends on laser irradiation parameters such as power, and image size as well as absorption and scattering properties of tissues. This paper analyzes, using finite element modeling, photo-thermal heating of tumor in the presence of intravenous blood injection or intratumorally injected gold nanorods. The Pennes bio-heat transfer equation was solved to compute temperature evolution. A volumetric heat generation based on Beer-Lambert law was used to model the laser heating. The predicted temperatures at the tumor surface were compared with available experimental results and are found to be good. To determine the efficacy of intratumoral injection of nanoparticles, a comparative study was also carried out to investigate the tumor thermal history for both the blood injection and targeted injection. Thermal damage of the tumor tissue was predicted by virtue of denaturation of single protein. It was found that a significant protein denaturation occurs when the temperature reaches around 53° C. A parametric study using the numerical model was also performed to quantify the effects of size and depth of the tumor, laser power and the concentration of the nanoparticles. Following intratumoral targeted injection; the computational heat transport modeling can be used to predict photo-thermal heating during laser irradiation.

## 1. INTRODUCTION

Photo-thermal therapy is the use of electromagnetic (EM) radiation, most often in the near infrared region to treat various medical conditions, including cancer. The basic model for its use is derived in part from photo-dynamic therapy, in which a photosensitizer is excited with specific band of light. This activation brings the sensitizer to an excited state where it releases vibrational energy resulting in heating which is used to kill the targeted tumor cells. Photo-thermal therapy does not require oxygen to interact with the target cells or tissues. Current studies [1, 2] also show that photo-thermal therapy is able to use longer wavelength light, which is less energetic and therefore less harmful to other cells and tissues.

Photo-thermal ablative tumor therapies have the potential to provide a robust, generalized method of cancer treatment. However, traditional methods for delivering external energy to tumors lack specificity. Thermal ablation by laser [3–6] is useful for external tumors but when the tumor gets deeply rooted, high frequency EM wave laser destroys the background tissue and water content and thus becomes ineffective. The electromagnetic properties of plasmonic nanomaterials have been harnessed to develop ultrasensitive diagnostic [7]. Gold nanorods (NRs) have been used for a diversity of biological purposes. In addition to their plasmon resonance, the larger atomic number and high material density of gold nanomaterials compared with clinical formulations of iodine-based reagents have

---

\*Corresponding Author: Ph No: +91-4422574655, E-mail address: skdas@iitm.ac.in

attracted interest for X-ray computed tomography (CT) angiography. Spherical nanoparticle reagents have been developed for in vivo use [8, 9]. Mathematical modeling of photo-thermal therapy [10] was carried out with the tumor assumed to be of ellipsoid shape with uniform distribution of gold NRs. By tuning the nanoshells it is intended to absorb light strongly in the near infrared range [3], where optical transmission through tissue is optimal. The distribution of nanoshells at depth in tissues can be used to deliver a therapeutic thermal dose by using moderately low exposures of extra corporeally applied near-infrared (NIR) light. Nanoshells also possess tunable optical properties [11] in the NIR region to provide optical contrast for improved diagnostic imaging of tumor and, at higher light intensity, rapid heating for photo-thermal therapy. The properties of the nanoshells [12] are dependent on their preparation and are used to increase the photo-thermal temperature of tissue phantom. Plasmonic nanoantennas [13] have an opportunity to alter this paradigm by targeting tumors and capturing externally applied near-infrared energy for localized photo-thermal ablation. The electromagnetic properties of plasmonic nanomaterials have been harnessed to develop therapeutic technologies. In particular, tunable plasmonic nanomaterials have attracted attention for their immense optical absorption coefficients and potential as injectable nanoantennas that target tumors and locally convert electromagnetic energy to thermal energy for ablation.

The whole anatomical structure of biological tissue can contain vascular networks of different sizes. The size of the vascular networks can vary from few microns to a few millimeters. When the size of blood vessels are greater than 500  $\mu\text{m}$  [14-16] they are called as large blood vessels and the energy transport equations for tissue and blood in such large blood vessels must be treated separately. The cooling effect caused by tissue blood perfusion in micro capillaries can remove significant amount of the energy during laser irradiation. A classical Pennes [17] bio heat equation is well accepted energy equation which takes care of the blood flow through micro capillaries. Fujita et al. [18] has described the effect of blood perfusion and its temperature dependency on tumor ablation during radio-frequency capacitive hyperthermia.

This paper describes the development of a system for improved photo-thermal tumor therapy, comprising of computational photo-thermal modeling consisting of laser heating modeled by Beer-Lambert law. A different blood perfusion rate was considered for the tissue and the tumor along with its dependency on temperature. Two types of nanoparticle injection strategy to the tumor site *viz.* intratumoral injection and intravenous injection of gold NRs were discussed. The tissue damage parameter was also calculated to determine the efficacy of localized injection of nanoparticles to the tumor site over intravenous blood injection. In the later part of the study, the effects of laser parameter, tumor specification and nanoparticle concentration were calculated and discussed. Following intratumoral targeted injection of gold Nrs; the computational heat transport modeling can be used to predict photo-thermal heating during laser irradiation, which can be useful to optimize tunable parameters during photo-thermal therapy.

## 2. MATHEMATICAL MODEL

To obtain the thermal history a finite element modeling was carried out. The bio-heat transfer equation of Pennes [17] which was designed to model heat transfer within tissue was applied to the computational domain in the form:

$$(\rho C) \frac{\partial T}{\partial t} = \nabla \cdot (k \nabla T) + Q_{blood} + Q_{met} + Q_{source}(r, z) \quad (1)$$

$$Q_{blood} = \rho_b \omega_b C_b (T_b - T) \quad (2)$$

The temperature and location dependence of the blood perfusion rate can be written as,

$$\omega_b = \omega_b(F, T, P) \quad (3)$$

Table 1. Details of coefficients pertinent to temperature dependent blood perfusion [18]

Tissue	F [m <sup>3</sup> /kg/s]	P	$\omega_b$
Tumor core	$5 \times 10^{-7}$	1.0	= F[1] for T ≤ 39 °C
Tumor periphery	$1.67 \times 10^{-6}$	2.0	= F[1+(P-1)(T-39)/6] for 39 °C < T ≤ 45 °C
Muscle	$8.3 \times 10^{-6}$	9.0	= F[P-(P-1)(T-45)/6] for 45 °C < T ≤ 51 °C
Skin	$8.3 \times 10^{-6}$	9.0	= F[1] for T ≥ 51 °C

Table 2. The thermo physical properties of various regions [10]

Tissue	Density [kg/m <sup>3</sup> ]	Specific heat [J/kg K]	Thermal conductivity [W/m K]
Tumor core	1050	3700	0.5
Tumor periphery	1050	3700	0.5
Muscle	1050	3700	0.5
Skin	1200	3700	0.2
Blood	1000	4200	0.6
Gold NRs	18900	130	318

The maximum perfusion rate F and the parameter P for different region are given as in Table 1 [18]. The thermo physical properties of various regions were taken from accepted values as shown in Table 2 [10]. The metabolic heat generation rate ( $Q_{met}$ ) was taken as 400 W/m<sup>3</sup> [10].

The light-tissue interaction is highly dependent on the wavelength of light. Blood and water are major absorbers of light in visible and infrared region respectively and hence the best spectral window used for the photo-thermal therapy is the NIR window at which tissue transmissivity is highest. In this study, an 810 nm [10] wavelength laser was considered. The laser heat generation in tissues is a widely studied area and a good review of various models [19] is available in the literature. Assuming light distribution inside the tissue to be due to a Gaussian beam the following equation for heat generation appears to be an appropriate choice;

$$Q_{source}(r, z) = \kappa I_0 \exp\left\{\frac{-r^2}{(2\sigma^2(0)\exp(\sigma_s z))}\right\} \exp\{-(\kappa + \sigma_s)z\} \quad (4)$$

## 2.1. Initial and boundary conditions

Initial condition:

$$T(r, z, 0) = 34^\circ\text{C} \quad (5)$$

Skin surface:

$$(k_s \nabla T) = h.(T_{amb} - T) \quad (6)$$

All other boundaries:

$$(k \nabla T) = 0 \quad (7)$$

The surface convective heat loss coefficient to ambient was taken as 10 W/m<sup>2</sup>K [10], which is a typical value for natural convection on planar surfaces. The ambient temperature ( $T_{amb}$ ) was considered as 25 °C.

## 2.2. Damage integral calculation

To find out the magnitude of thermal damage in a living tissue, a damage parameter ( $\Omega$ ) is given by [19];

$$\Omega = \ln\left(\frac{C_0}{C_0 - C_d}\right) \quad (8)$$

where  $C_0$  is the protein concentration in non-irradiated tissue and  $C_d$  is the concentration of damaged protein. The complete cellular necrosis occurs at  $\Omega \geq 1$ . The thermal damage of the tumor tissue based on obtained temperature history during therapy can be calculated using Arrhenius equation. The rate of thermal damage is given as

$$\frac{d\Omega}{dt} = A \exp\left(\frac{-E}{RT}\right) \quad (9)$$

Where  $A$  = pre-exponential factor, which was taken as  $3.1 \times 10^{98} \text{ s}^{-1}$ ,  $E$  = activation energy for the reaction and its value was taken as  $6.28 \times 10^5 \text{ J/mol}$  [19],  $\bar{R}$  = Universal gas constant (J/mol K),  $T(r,z,t)$  = Temperature (K). The activation energy and pre-exponential factor is related to the entropy change  $\Delta S$  [20]

$$A = \frac{k_B T}{h} \exp\left(\frac{\Delta S}{R}\right) \quad (10)$$

where,  $h$  is the Plank constant and  $k_B$  is the Boltzman constant,  $\Delta S$  can be obtained from  $A$  through

$$\Delta S = \bar{R} \ln\left\{\frac{(A \times h)}{(k_B \times T)}\right\} \quad (11)$$

The above model has been used by the researchers [19, 20] to determine the tissue thermal injuries.

## 3. COMPUTATION AND VALIDATION

To understand the magnitude and kinetics of in vivo photo-thermal heat generation by the nanorods and native tissue, the temporal and spatial propagation of thermal gradients, and to assess the timescale within which the entire tumor volume would reach ablative temperatures, a finite element computer simulation of the photo-thermal ablation process was carried out. The tumor was approximated as an ellipsoid of size 6 mm along the minor axis and 8 mm along major axis resting above the muscle and covered by skin of 300  $\mu\text{m}$  thickness. For modeling, muscle was considered as a cylinder of 30 mm diameter surrounding the tumor with a depth of 20 mm for the computation. In case of targeted injection, the gold NRs are assumed to be injected into a shell of circular cross-section with diameter of 1 mm at the tumor core, so that nanorods are concentrated at the tumor core. The optical properties of gold NRs are considered as per reference [21]. However, in case of intravenous injection, the gold NRs are assumed to be uniformly distributed in the tumor region only. In this case, the optical properties of tumor are considered as per reference [10]. When the laser is irradiated on the tumor the

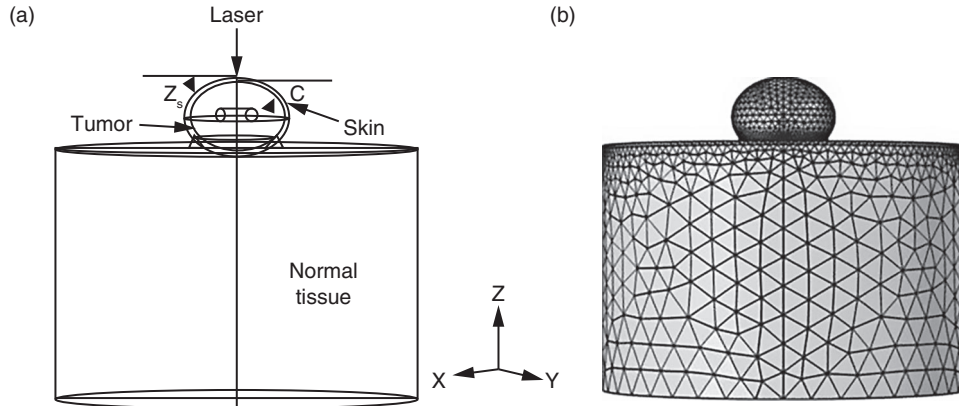


Figure 1. (a) Geometry used for laser irradiation (b) computational model after meshing

photo-thermal heat will be concentrated only at the tumor because of higher absorptivity of the gold NRs. Whenever tumor reaches the ablative temperatures, it will be destructed. The spot size of the laser used here was a circular beam of diameter 7 mm [10].

The Pennes bio-heat transfer eqn (1) is solved with eqns (2-7). However, eqn (4) is valid only if the radiation is falling on a planar skin at  $z = 0$  and the absorption and scattering coefficients of various layers are identical. Obviously this is not the case with nanorod absorption where the tumor is projected and it attains a higher absorptivity. This gives rise to a discontinuity in laser beam attenuation within various layers (skin and tumor). This can be incorporated by modifying the above equation as [10]

$$Q_{source}(r, z) = \kappa I_0 \exp\left\{\frac{-r^2}{(2\sigma^2(0)\exp(\sigma_s z_c))}\right\} \exp\{-(\kappa + \sigma_s)(z_c - c - d)\} \exp\{-(\kappa + \sigma_s)(z_s)\} \exp\{-(\kappa + \sigma_s)(z_t)\} \quad (12)$$

here,  $c$  is the depth of the skin surface from the tumor vertex at a given radial position,  $d$  is the depth of the normal tissue above a location,  $z_s$  is the depth of the skin above a location and  $z_t$  is the depth of the tumor tissue above a location as shown in Fig. 1(a). This incorporates differential beam attenuation in different layers.

The finite element method (FEM) using the multiphysics enabled software COMSOL 4.3 (Burlington, MA) was used for modeling. First a coarse mesh containing 41686 tetrahedral elements was applied for the domain. Then the mesh was changed to fine containing 81467 elements and finally to finer mesh containing 186256 elements. When the coarse mesh was changed to fine mesh, the solution was changed by 0.541%, whereas when it was changed from fine to finer mesh the solution was changed by 0.031%. The solution time increased by 96% for the first case and by 122% in the second case. It was clear that the solution was quite grid independent so the solution with fine meshes was continued. The meshed model is shown in Fig. 1(b). The temperature tolerance of 0.0001 and a direct matrix inversion technique was used. The simulated maximum surface temperature was compared with the experimental trends and simulated X-Ray tomography data obtained by von Maltzahn et al. [10] as shown in Fig.2. In a representative set of experiments on mice bearing MDA-MB-435 tumors on opposing flanks, the animals were irradiated with 810 nm diode laser and the tumor surface temperature were measured using thermographic equipment.

#### 4. RESULTS AND DISCUSSION

During hyperthermia treatment any temperature in the range of 41-44 °C is sufficient for protein denaturation and cells die at a temperature of about 50-100 °C for laser heating period of few

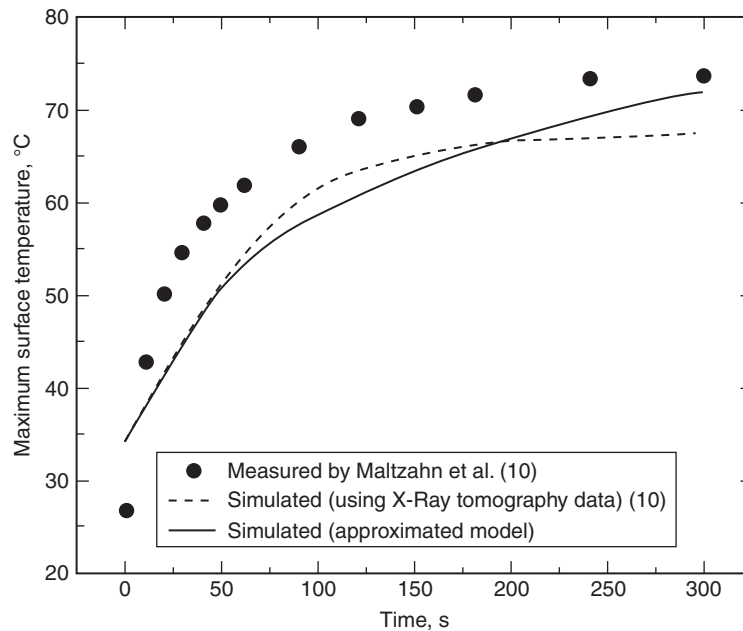


Figure 2. Maximum tumor surface temperature vs. time. The circular dots shows experimentally measured temperature [10]. The dashed line shows the simulated X-Ray tomography data [10]. The solid line represents the computational results of the approximated model ( $0.75\text{W}/\text{cm}^2$ ,  $2.5 \times 10^{18} \text{m}^{-3}$ )

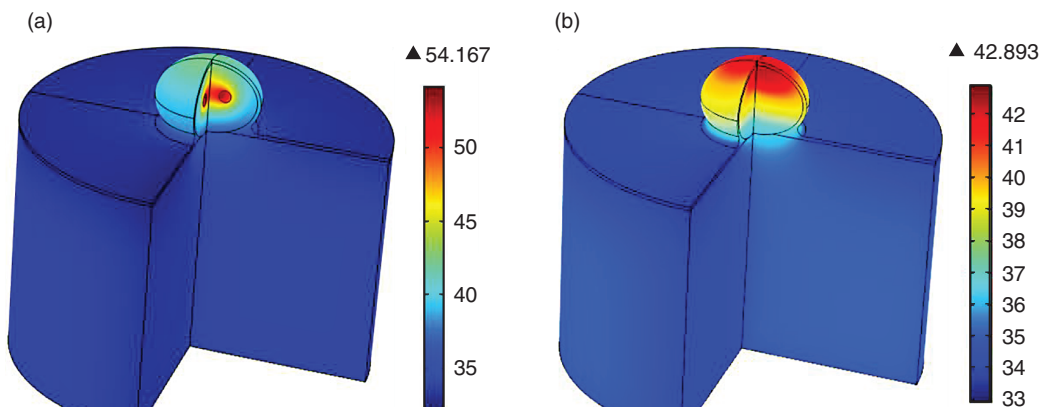


Figure 3. At  $t = 60$  sec after the onset of laser: Temperature distribution within the complete computational domain (a) for intratumoral injection. (b) for intravenous injection ( $0.75 \text{W}/\text{cm}^2$ ,  $2.5 \times 10^{18} \text{m}^{-3}$ )

seconds [22,23]. To understand the thermal effect of laser heating of tumor embedded with gold NRs, the Pennes bio-heat equation was solved for the approximated computational domain (Fig.1) and the simulation results are shown in Fig.3. The maximum temperature observed in the tumor core is  $54.2^\circ\text{C}$  and the top surface of the tumor has reached around  $45^\circ\text{C}$  in case of intratumoral injection of gold NRs which is sufficient for the tumor necrosis. However, a different thermal profile has been obtained in the case of intravenous injection of nanoparticles. In this case, a temperature of  $43^\circ\text{C}$  has been obtained in the top half of the tumor and the bottom half has reached only  $39^\circ\text{C}$  which is insufficient for the complete tumor necrosis. Figure 4 depicts the tumor core temperature after 300s of laser irradiation for

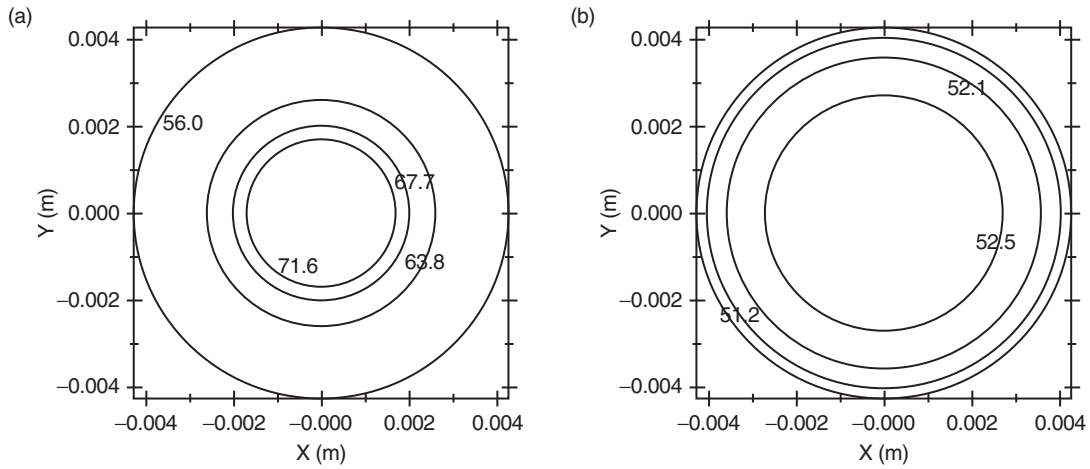


Figure 4. Temperature isotherms in °C at XY-plane ( $0.75\text{W/cm}^2$ ,  $2.5 \times 10^{18}\text{m}^{-3}$  and 300s) at tumor core for a) intratumoral injection of gold NRs (b) intravenous injection of gold NRs

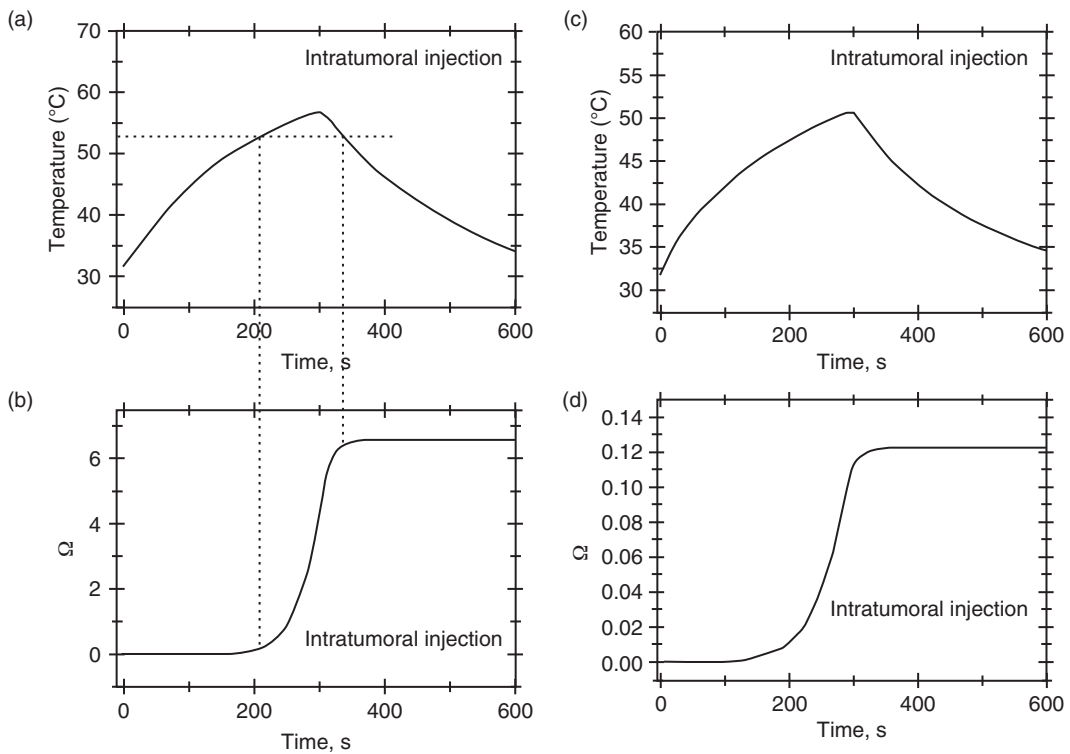


Figure 5. Prediction of temperature ((a) and (c)) and damage integral ((b) and (d)) at tumor periphery ( $r = 4 \text{ mm}$  and  $z = 3.3 \text{ mm}$ ) as a function of time ( $0.75 \text{ W/cm}^2$ ,  $2.5 \times 10^{18}\text{m}^{-3}$ )

both the case of intratumoral and intravenous injection of gold NRs. This gives an impression of the advantage of intratumoral injection of nanoparticles to the tumor site over intravenous injection. Figure 5 depicts the temperature and damage parameter at tumor periphery adjacent to the nanoparticle zone ( $r = 4 \text{ mm}$  and  $z = 3.3 \text{ mm}$ ). In this case, the laser power intensity was taken as  $0.75 \text{ W/cm}^2$ , beam radius

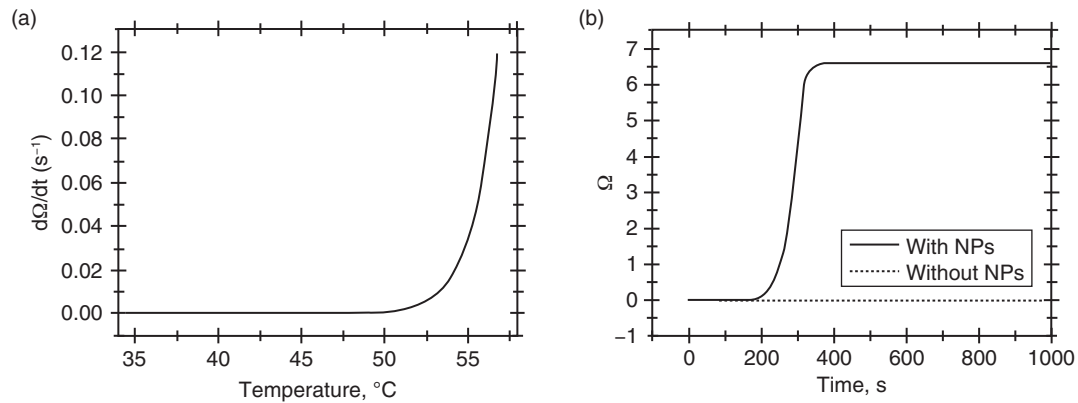


Figure 6. Damage accumulation rate ( $d\Omega/dt$ ) vs. temperature (a) and comparison of damage parameter as a function of time between with and without introducing Gold NPs (b) at tumor periphery ( $r = 4$  mm and  $z = 3.3$  mm) ( $0.75$  W/cm<sup>2</sup>,  $2.5 \times 10^{18}$ m<sup>-3</sup>). In the case of intratumoral injection

of  $0.0035$  m, exposure time of  $300$  s and then allowed to cool up to another  $300$  s. The temperature increases with increase in time till the laser is switched off and then comes down due to the diffusion of heat to the neighboring healthy tissues.

The damage parameter is very low until the temperature rises to about  $53$  °C as shown in Fig. 5 (a and b) and then a steep rise is observed till the laser is turned off. There is a continuous increase in damage parameter even after the laser is turned off till the temperature comes down to  $53$  °C and afterwards it becomes perpetual. The predicted damage parameter beyond  $53$  °C is  $> 1$  [19] and hence sufficient for the irreversible damage. While, a damage parameter of  $0.12$  is observed in the case of intravenous injection of nanoparticles. Also the damage accumulation rate ( $d\Omega/dt$ ) is negligible below the temperature of  $53$  °C and it increases abruptly when temperature passed  $53$  °C as shown in Fig.6 (a). Figure 6(b) illustrates the extent of tissue damage between the cases of with and without introducing Gold NPs. It is seen that the presence of NPs in the tumor domain results in local irreversible damage to the tumor tissue.

Parametric study is helpful in better understanding ablative tumor therapy. It is also useful in deciding the laser energy to be irradiated for fixed duration of time, for a particular size of the tumor located at a particular depth. For example if the tumor is located at a depth far away from the skin, the laser heat causes significant damage to the healthy tissue before it reaches the targeted tumor. This therapy should not be used in such cases as the thermal damage to the healthy tissue is high. Similarly if a large size tumor is located just below the skin, the laser spot size required for tumor ablation is also large. Parametric study was carried out for the case of intratumorally injected gold NPs because of its high efficacy in tumor necrosis by running the simulations by varying the parameter under study keeping the other parameters constant. The main parameters which affect the temperature distribution within the tumor are concentration of the nanorods, depth of the tumor below the skin, intensity of the laser and size of the tumor.

The absorption coefficient ( $\kappa$ , m<sup>-1</sup>) quantifies how much absorption is completed to the incident light per unit depth of tissue. The absorption coefficient of gold NRs was calculated with an effective size of  $11.43$  nm for different concentration ( $n$ ). The predicted temperature variation for the computational domain is shown in Fig.7 (a) and Fig.7 (b), which symbolize that the tumor temperature increases linearly with the increase in gold NRs concentration. This is because the enhancement of NRs concentration leads to the increase in the absorption coefficient of the tumor, which give rise to an increase in the temperature ( $T_a$ ) (Temperature at tumor periphery below the laser spot at  $r = 0$  mm and  $z = 300$  μm) and ( $T_b$ ) (Temperature at tumor periphery adjacent to the nanoparticle

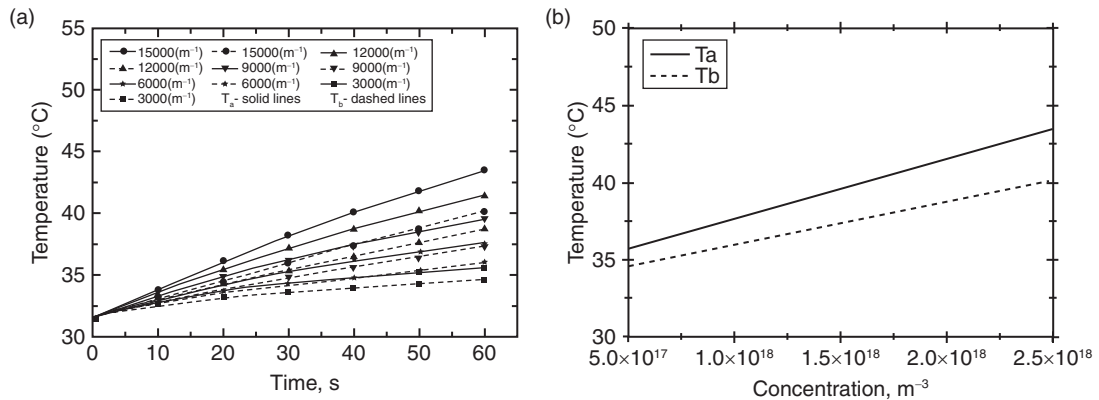


Figure 7. Effect of Gold NRs concentration on temperature at two different points ( $T_a$  and  $T_b$ ) on the tumor surface ( $0.75 \text{ W/cm}^2$  and  $60\text{s}$ )

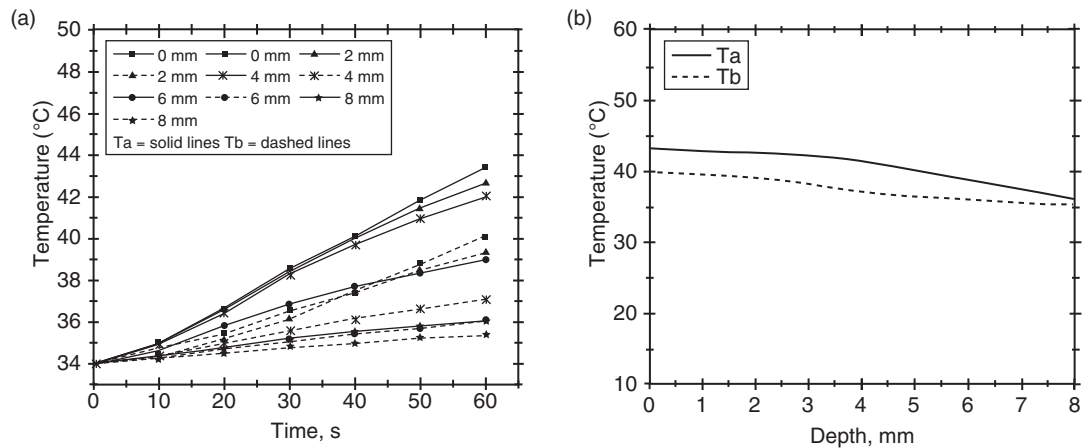


Figure 8. Effect of tumor depth below the skin on temperature at two different points ( $T_a$  and  $T_b$ ) on the tumor surface ( $0.75 \text{ W/cm}^2$ ,  $2.5 \times 10^{18} \text{ m}^{-3}$  and  $60\text{s}$ )

zone at  $r = 4 \text{ mm}$  and  $z = 3.3 \text{ mm}$ ) from  $35 \text{ }^\circ\text{C}$  to  $40 \text{ }^\circ\text{C}$  for a heating period of 60 seconds. When the depth of the tumor below the skin increases, the temperature (both  $T_a$  and  $T_b$ ) decreases as shown in Fig.8. This is because of the fact that the scattering coefficient of the muscle part above the tumor is higher than its absorption coefficient. So, the laser irradiation which reaches the tumor is less as most of it part is scattered by this muscle part. The change in temperature with different laser power is shown in Fig.9. As the laser power increases, the temperature also increases linearly. This is quite conclusive that the temperature would increase rapidly when the laser power is higher and this rapid temperature rise helps in early tumor ablation. With the increase in the tumor size, the temperature increases up to certain size of the tumor and then it decreases (Fig.10a). With the increase in the tumor size, the amount of nanorods to be injected increases proportionately, the heat absorption also increases which causes the increase in temperature. But, a further increase in tumor size causes increase in the surface area exposed to outside atmosphere. Hence, the amount of heat loss by convection to the surrounding also increases. Therefore, beyond 4.5 mm of tumor height the surface temperature drops approximately by  $5 \text{ }^\circ\text{C}$  (Fig.10b) since the amount of heat absorption is less than the amount of heat loss by convection.

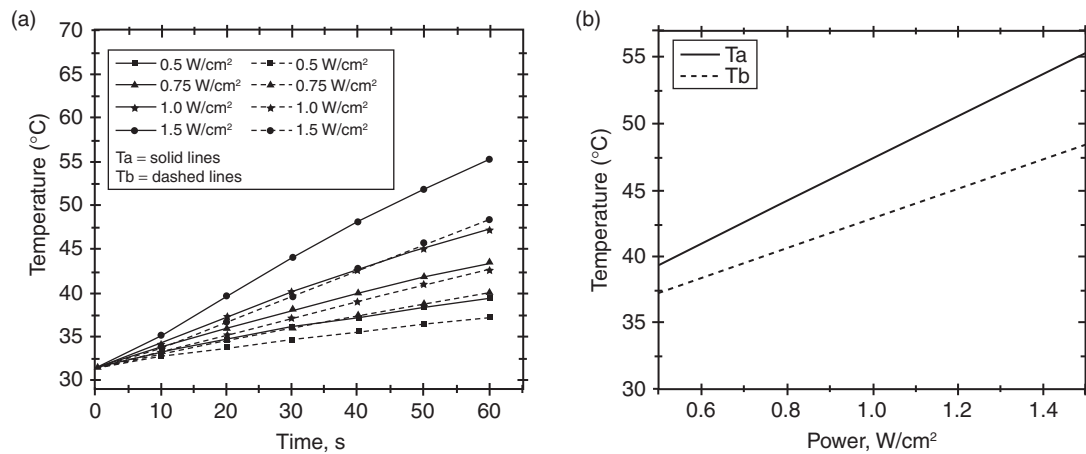


Figure 9. Effect of laser power on temperature at two different points ( $T_a$  and  $T_b$ ) on the tumor surface ( $0.75 \text{ W/cm}^2$ ,  $2.5 \times 10^{18} \text{ m}^{-3}$  and 60s)

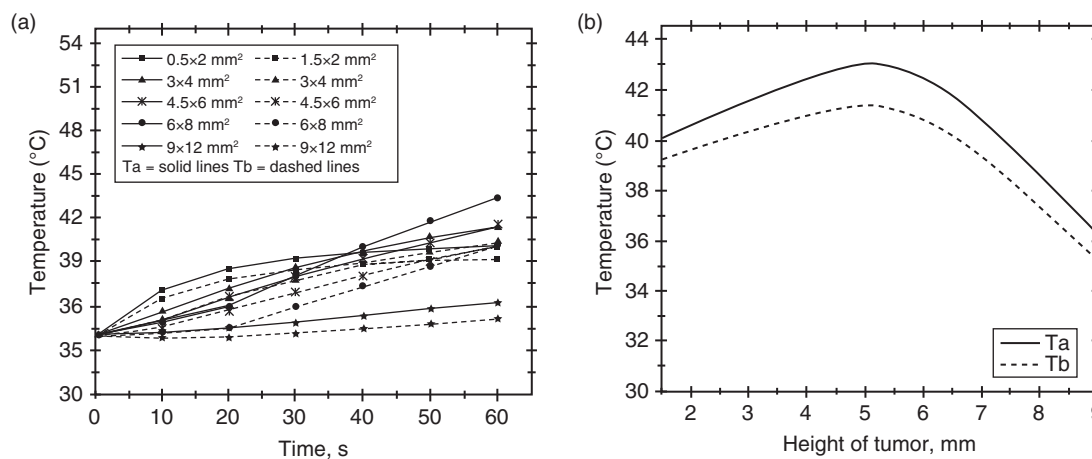


Figure 10. Effect of tumor size on temperature at two different points ( $T_a$  and  $T_b$ ) on the tumor surface ( $0.75 \text{ W/cm}^2$ ,  $2.5 \times 10^{18} \text{ m}^{-3}$  and 60s)

## 5. CONCLUSIONS

The present study on localized injection of nanoparticles to tumor site has shown that photo-thermal computational modeling to guide surgical irradiation planning is feasible. The temperature history and the sub-surface tumor temperature distribution revealed by the simulation indicate enhancement of photo-thermal heating due to the presence of nanoparticles. The nanoparticles also enable substantial thermal gradients near the tumor volume which causes a irreversible damage. Two types of targeting strategy of nanoparticles viz. intratumoral injection and intravenous blood injection to the tumor site has been discussed and subsequently intratumoral injection has been found appropriate for the complete tumor necrosis. A significant protein denaturation occurs when the tumor temperature reaches around  $53 \text{ }^\circ\text{C}$ . The subsequent parametric study results provide the critical irradiation parameters to be used for ablation of a tumor of fixed size located at a particular depth. When the tumor is of bigger size

( $\geq 4.5$  mm) and also deeply rooted ( $\geq 4$  mm), the temperature resulting from laser heating is not sufficient ( $\leq 40$  °C) for the complete necrosis. This mathematical model highlights the potential of fusing computational design with nano-therapeutic development for ultra-selective tumor ablation.

### NOMENCLATURE

$\rho$	Density, kg/m <sup>3</sup>
$C$	Specific heat, J/kg K
$k$	Thermal conductivity, W/m K
$T$	Temperature, K
$t$	Time, s
$I$	Laser intensity, W/m <sup>2</sup>
$r, z$	Space coordinates, m
$Q_{blood}$	Heat transfer due to blood perfusion, W/m <sup>3</sup>
$Q_{source}$	Laser heat generation, W/m <sup>3</sup>
$Q_{met}$	Metabolic heat generation, W/m <sup>3</sup>
$C_o$	Protein concentration in non-irradiated tissue
$C_d$	Concentration of damage protein
$A$	Pre-exponential factor, s <sup>-1</sup>
$E$	Activation energy, J/mol
$\omega$	Perfusion rate, s <sup>-1</sup>
$\Omega$	Damage integral
$R$	Universal gas constant, J/mol K
$h$	Heat transfer coefficient, W/m <sup>2</sup> K

### Greek Symbols

$\kappa$	Absorption coefficient, m <sup>-1</sup>
$\sigma$	Gaussian beam distribution
$\sigma_s$	Scattering coefficient, m <sup>-1</sup>

### Subscripts

0	Skin surface (0,0)
S	Skin
b	Blood
amb	Ambient

### REFERENCES

- [1] E. B. Dickerson, E. C. Dreaden, X. Huang, I. H. El-Sayed, H. Chu, S. Pushpanketh, J. F. McDonald, and M. A. El-Sayed, "Gold nanorod assisted near-infrared plasmonic photothermal therapy (ppt) of squamous cell carcinoma in mice," *Cancer Letters*, 2008, 269(1), 57–66.
- [2] G. von Maltzahn, A. Centrone, J. H. Park, R. Ramanathan, M. J. Sailor, T. A. Hatton, and S. N. Bhatia, "Sers-coded gold nanorods as a multifunctional platform for densely multiplexed near-infrared imaging and photothermal heating," *Advanced Materials*, 2009, 21(31), 3175–3180.
- [3] L. R. Hirsch, R. J. Stafford, J. A. Bankson, S. R. Sershen, B. Rivera, R. E. Price, J. D. Hazle, N. J. Halas, and J. L. West, "Nanoshell-mediated near-infrared thermal therapy of tumors under magnetic resonance guidance," *Proceedings of the National Academy of Sciences*, 2003, 100(23), 13549–13554.
- [4] X. Huang, I. H. El-Sayed, W. Qian, and M. A. El-Sayed, "Cancer cell imaging and photothermal therapy in the near-infrared region by using gold nanorods," *Journal of the American Chemical Society*, 2006, 128(6), 2115–2120.
- [5] R. S. Norman, J. W. Stone, A. Gole, C. J. Murphy, and T. L. Sabo-Attwood, "Targeted photothermal lysis of the pathogenic bacteria, *pseudomonas aeruginosa*, with gold nanorods," *Nano Letters*, 2008, 8(1), 302–306.

- [6] D. O'Neal, L. R. Hirsch, N. J. Halas, J. Payne, and J. L. West, "Photo-thermal tumor ablation in mice using near infrared-absorbing nanoparticles," *Cancer Letters*, 2004, 209(2), 171–176.
- [7] R. Elghanian, J. J. Storhoff, R. C. Mucic, R. L. Letsinger, and C. A. Mirkin, "Selective colorimetric detection of polynucleotides based on the distance-dependent optical properties of gold nanoparticles," *Science*, 1997, 277(5329), 1078–1081.
- [8] D. Kim, S. Park, J. H. Lee, Y. Y. Jeong, and S. Jon, "Antibiofouling polymer-coated gold nanoparticles as a contrast agent for in vivo x-ray computed tomography imaging," *Journal of the American Chemical Society*, 2007, 129(24), 7661–7665.
- [9] Q. Cai, S. Kim, K. Choi, S. Kim, S. Byun, K. Kim, S. Park, S. Juhng, and K. Yoon, "Colloidal gold nanoparticles as a blood-pool contrast agent for x-ray computed tomography in mice," *Investigative Radiology*, 2007, 42(12), 797–806.
- [10] G. von Maltzahn, J. H. Park, A. Agrawal, N. K. Bandaru, S. K. Das, M. J. Sailor, and S. N. Bhatia, "Computation-ally guided photothermal tumor therapy using long-circulating gold nanorod antennas," *Cancer Research*, 2009, 69(9), 3892–3900.
- [11] A. M. Gobin, M. H. Lee, N. J. Halas, W. D. James, R. A. Drezek, and J. L. West, "Near-infrared resonant nanoshells for combined optical imaging and photothermal cancer therapy," *Nano Letters*, 2007, 7(7), 1929–1934.
- [12] S. Lal, S. E. Clare, and N. J. Halas, "Nanoshell-enabled photothermal cancer therapy: Impending clinical impact," *Accounts of Chemical Research*, 2008, 41(12), 1842–1851.
- [13] D. DasGupta, G. Von Maltzahn, S. Ghosh, S. N. Bhatia, S. K. Das, and S. Chakraborty, "Probing nanoantenna-directed photothermal destruction of tumors using noninvasive laser irradiation," *Applied Physics Letters*, 2009, 95(23), 233701–233701–3.
- [14] J. Crezee, J. J. W. Lagendijk, "Temperature uniformity during hyperthermia: the impact of large vessels," *Physics in Medicine and Biology*, 1992, 37, 1321.
- [15] L. Consiglieri, dos Santos, I., D. Haemmerich, "Theoretical analysis of the heat convection coefficient in large vessels and the significance for thermal ablative therapies," *Physics in Medicine and Biology*, 2003, 48, 4125
- [16] A. Paul, A. Narasimhan, F. J. Kahlen, S. K. Das, "Temperature evolution in tissues embedded with large blood vessels during photo-thermal heating," *Journal of Thermal Biology*, 2014, 41, 77–87.
- [17] H. Pennes, "Analysis tissue and arterial temperatures in the resting human forearm," *Journal of Applied Physiology*, 1948, 1(1), 93–122.
- [18] S. Fujita, M. Tamazawa, and K. Kuroda, "Effects of blood perfusion rate on the optimization of rf-capacitive hyperthermia," *IEEE Transactions on Biomedical Engineering*, 1998, 45(9), 1182–1186.
- [19] A. Welch, "The thermal response of laser irradiated tissue," *IEEE Journal of Quantum Electronics*, 1984, 20(12), 1471–1481.
- [20] F. C. Henriques, "Studies of thermal injur," *Arch. Patho*, 1947, 43, 489.
- [21] P. K. Jain, K. S. Lee, I. H. El-Sayed, and M. A. El-Sayed, "Calculated absorption and scattering properties of gold nanoparticles of different size, shape, and composition: Applications in biological imaging and biomedicine," *Journal of Physical Chemistry B*, 2006, 110, pp. 7238–7248.
- [22] K. P. Ritchie, B. M. Keller, K. M. Syed, and J. R. Lepock, "Hyperthermia (heat shock)-induced protein denatura-tion in liver, muscle and lens tissue as determined by differential scanning calorimetry," *International Journal of Hyperthermia*, 1994, 10(5), 605–618.
- [23] D. M. Simanovskii, M. A. Mackanos, A. R. Irani, C. E. O'Connell-Rodwell, C. H. Contag, H. A. Schwettman, and D. V. Palanker, "Cellular tolerance to pulsed hyperthermia," *Physical Review E*, 2006, 74, 011915.